BIOCHEMISTRY
including biophysical chemistry & molecular biology

Article

pubs.acs.org/biochemistry

Terms of Use

Covalent Small Molecule Inhibitors of Ca^{2+}-Bound S100B

Michael C. Cavalier,[†] Adam D. Pierce,[†] Paul T. Wilder,[†,‡] Milad J. Alasady,[†] Kira G. Hartman,[†] David B. Neau,[§] Timothy L. Foley,[∥] Ajit Jadhav,[∥] David J. Maloney,[∥] Anton Simeonov,[∥] Eric A. Toth,[†,‡] and David J. Weber*[,†,‡]

[†]Center for Biomolecular Therapeutics (CBT), Department of Biochemistry and Molecular Biology, University of Maryland School of Medicine, Baltimore, Maryland 21201, United States

[‡]Marlene and Stewart Greenebaum Cancer Center, University of Maryland School of Medicine, Baltimore, Maryland 21201, United States

[§]NE-CAT, Cornell University, Argonne, Illinois 60439, United States

[∥]National Center for Advancing Translational Sciences, National Institutes of Health, Bethesda, Maryland 20892, United States

Supporting Information

ABSTRACT: Elevated levels of the tumor marker S100B are observed in malignant melanoma, and this EF-hand-containing protein was shown to directly bind wild-type (wt) p53 in a Ca^{2+}-dependent manner, dissociate the p53 tetramer, and inhibit its tumor suppression functions. Likewise, inhibiting S100B with small interfering RNA ($siRNA^{S100B}$) is sufficient to restore wild-type p53 levels and its downstream gene products and induce the arrest of cell growth and UV-dependent apoptosis in malignant melanoma. Therefore, it is a goal to develop S100B inhibitors (SBi*X*s) that inhibit the S100B−p53 complex and restore active p53 in this deadly cancer. Using a structure−activity relationship by nuclear magnetic resonance approach (SAR by NMR), three persistent binding pockets are found on S100B, termed sites 1−3. While inhibitors that simultaneously bind sites 2 and 3 are in place, no molecules that simultaneously bind all three persistent sites are available. For this purpose, Cys84 was used in this study as a potential means to bridge sites 1 and 2 because it is located in a small crevice between these two deeper pockets on the protein. Using a fluorescence polarization competition assay, several Cys84-modified S100B complexes were identified and examined further. For five such SBi*X*−S100B complexes, crystallographic structures confirmed their covalent binding to Cys84 near site 2 and thus present straightforward chemical biology strategies for bridging sites 1 and 3. Importantly, one such compound, SC1982, showed an S100B-dependent death response in assays with WM115 malignant melanoma cells, so it will be particularly useful for the design of SBi*X* molecules with improved affinity and specificity.

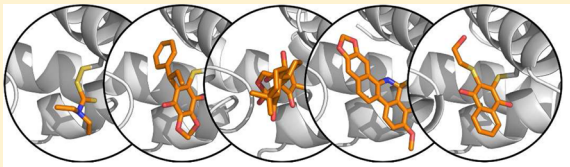

Covalent small molecule inhibitors of Ca^{2+}-bound S100B

Despite improvements in chemotherapy, BRAF/MEK inhibitors, cytokine treatments, immunotherapies, vaccines, and combinatorial approaches for treating malignant melanoma (MM),[1−5] long-term survival (>3 years) remains very poor for a majority of patients (>70%), and side effects from these treatments are sometimes quite severe.[2,6,7] These issues are even more problematic after the onset of metastasis and/or when drug-resistant mechanisms arise.[5,8] As with many cancers, survival from MM is most promising when it is detected early, so the development of useful biomarkers for detection and more recently for personalized medicine approaches is ongoing.[9,10] One such marker, S100B, is especially important to monitor because its level is elevated in >90% of MM patients and its protein level correlates directly with poor survival (<1 year) and relapse, and it is especially predictive when used in combination with other diagnostic indicators.[11−13] On the other hand, for the few MM patients (5−10%) who have low levels of S100B, the MM vaccine is most effective at providing longer survival times.[14,15]

The S100B protein is a marker for melanoma, and when its level is elevated, it contributes to disease progression.[16,17] While the mechanism of elevated S100B levels toward MM progression is not fully understood, it contributes to lowering protein levels of the tumor suppressor p53 in a Ca^{2+}-dependent manner.[18,19] Specifically, p53 is sequestered by Ca^{2+}-bound S100B (^{Ca}S100B), its phosphorylation in the C-terminal negative regulator domain blocked,[20−23] its oligomerization disrupted,[19] and its degradation promoted.[18,19,24,25] Because p53 is typically wild-type in MM,[26,27] efforts are underway to specifically inhibit formation of the ^{Ca}S100B−p53 complex[16,28,29] and restore p53 levels, particularly in cases in which the cancer is resistant to kinase inhibitors or other therapeutic options.[30] As a proof of principle, blocking the ^{Ca}S100B-dependent effect on p53 via RNA interference or by small molecule inhibitors (also known as SBi*X*s) restores p53 protein levels and its tumor suppression activities, including UV-activated apoptosis.[17,18,31] One such inhibitor, pentamidine

Received: May 9, 2014
Revised: September 30, 2014
Published: September 30, 2014

 © 2014 American Chemical Society dx.doi.org/10.1021/bi5005552 | *Biochemistry* 2014, 53, 6628−6640

(also termed SBi1), entered stage II clinical trials for the treatment of relapsed or refractory malignant melanoma in patients with wild-type p53 and detectable S100B (www.clinicaltrials.gov, identifier NCT00729807). However, despite this promising line of inquiry, efficacy, specificity, and toxicity issues need to be improved significantly for SBi*X* lead molecules and warrant further investigation using drug design approaches.

In previous structure–function studies of S100B,[32−35] three persistent binding sites were identified in ^{Ca}S100B–target and ^{Ca}S100B–SBi*X* complexes (Figure 1). Site 1 interactions were first highlighted via the structure of ^{Ca}S100B bound to the C-terminal regulatory domain of p53,[20] while sites 2 and 3 were elucidated in the detailed characterization of the ^{Ca}S100B–SBi1 complex.[36] Here we describe a series of inhibitors, which occupy only the central binding site on ^{Ca}S100B (site 2) through a covalent attachment to Cys84. To fully characterize this binding site, a series of "site 2" ^{Ca}S100B–SBi*X* complexes were subjected to crystallization trials. Five new ^{Ca}S100B–SBi*X* complexes were identified (i.e., for ^{Ca}S100B–SC124, ^{Ca}S100B–SBi4172, ^{Ca}S100B–SC1982, and ^{Ca}S100B–SC1475). As a group, these "site 2" inhibitors display a meaningful effect in cellular assays on their own, but as discussed here, they also provide promise for defining how to link SBi*X* molecules bound in sites 1 and 3, as part of a new chemical scaffold, which can occupy all three persistent binding pockets within ^{Ca}S100B, simultaneously. These data also identify a common conformational change that occurs as a result of "site 2" occupation, which is necessary to consider in future therapeutic design efforts.

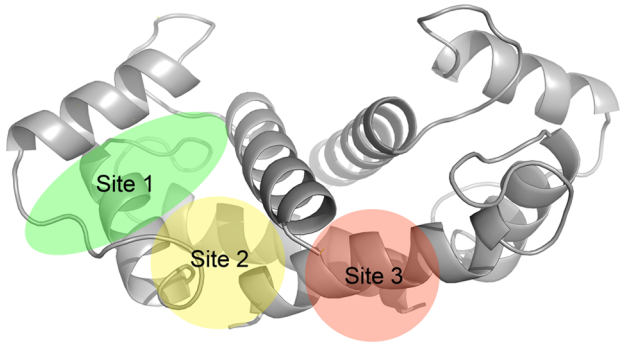

Figure 1. Binding sites 1–3. Shown is a ribbon diagram of the S100B dimer with the three persistent binding sites shaded. The sites were identified in ^{Ca}S100B–target and ^{Ca}S100B–SBi*X* complexes. Site 1 interactions were first highlighted via the structure of ^{Ca}S100B bound to the C-terminal regulatory domain of p53,[20] while sites 2 and 3 were elucidated in the detailed characterization of the ^{Ca}S100B–SBi1 complex.[36]

EXPERIMENTAL PROCEDURES

Purification. ^{15}N-labeled S100B (rat and bovine) was expressed and purified (>99%) with methods similar to those described previously.[37,38] The concentrations of S100B stock solutions were determined using the Bio-Rad Protein Assay (Bio-Rad Inc., Hercules, CA). The S100B was stored at a concentration of ∼10 mM in 0.25 mM Tris (pH 7.2) and 0.25 mM DTT at −20 °C until use.

Fluorescence Polarization Competition Assay (FPCA). The LOPAC1280 (Sigma-Aldrich) compound library was screened using an adaptation of a previously reported fluorescence polarization competition assay.[35] Briefly, the compounds were screened for binding to Ca^{2+}-loaded S100B by measuring changes in fluorescence polarization upon competition with the TAMRA-labeled version of peptide TRTK12, which is derived from CapZ protein residues 265–276 (TRTKIDWNKILS). The FPCA was performed in 0.2 μM S100B (rat), 25 nM TAMRA-TRTK12, 50 mM HEPES (pH 7.2), 100 mM KCl, 15 mM NaCl, 10 mM $CaCl_2$, 0.01% Triton X-100, and 0.3% DMSO in 1536-well plates with 8 μL per well.

NMR Spectroscopy. Purified ^{15}N-labeled S100B (rat) protein was dialyzed against 0.25 mM Tris (pH 7.5) and 0.25 mM DTT and concentrated to 10–15 mM using Amicon Ultra centrifugal filter units with a 10 kDa molecular weight cutoff; the concentration was determined using Bradford reagent (Bio-Rad), and protein was then aliquoted and stored at −20 °C. The Ca^{2+}-loaded S100B–SBi*X* heteronuclear single-quantum coherence (HSQC) samples contained 0.5 mM S100B subunit, 0.625 mM SBi*X*, 0.34 mM NaN_3, 15 mM NaCl, 5% DMSO-d_6, 10 mM $CaCl_2$, 10% D_2O, 0.2% TPEN, and 10 mM Hepes, adjusted to pH 7.2 with HCl. HSQC NMR data were collected at 37 °C with a Bruker Avance 800 US2 (800.27 MHz for protons) instrument equipped with pulsed-field gradients, four frequency channels, and triple-resonance, *z*-axis gradient cryogenic probes. Data were processed with NMRPipe, and proton chemical shifts were reported with respect to the H_2O or HDO signal taken as 4.608 ppm relative to external TSP (0.0 ppm). The ^{15}N chemical shifts were indirectly referenced as previously described using the following ratio of the zero-point frequency: 0.10132905 for ^{15}N to ^{1}H. A series of three-dimensional HNCA, HNCOCA, ^{15}N-edited NOESY-HSQC, and ^{15}N-edited HMQC-NOESY-HSQC NMR experiments were conducted, and the data were sufficient to unambiguously assign all the observable backbone ^{1}H, ^{15}N, and ^{13}C chemical shift values of S100B in the compound-bound state (Figures S1–S5 of the Supporting Information).

Crystallographic Studies. *Crystallization.* All crystallization experiments were conducted using vapor diffusion methods and performed as follows using purified ^{15}N-labeled S100B (bovine) protein. ^{Ca}S100B–SBi4172 crystals were grown in sitting drops consisting of a 0.75:0.75 μL protein solution [20 mg/mL S100B, 10 mM cacodylate (pH 7.2), 7.5 mM $CaCl_2$, and 2 mM SBi4172 prepared in DMSO-d_6] and mother liquor [20% 2-methyl-2,4-pentanediol, 0.1 M Hepes (pH 7.0), and 7.5 mM $CaCl_2$]. ^{Ca}S100B–SBi4434 crystals were grown in sitting drops consisting of a 0.75:0.75 μL protein solution [40 mg/mL S100B, 10 mM cacodylate (pH 7.2), 7.5 mM $CaCl_2$, and 4 mM SBi4434 prepared in DMSO-d_6] and mother liquor [40% 2-methyl-2,4-pentanediol, 0.1 M cacodylate (pH 6.0), and 7.5 mM $CaCl_2$]. ^{Ca}S100B–SC1982 crystals were grown in sitting drops consisting of a 0.75:0.75 μL protein solution [40 mg/mL S100B, 10 mM cacodylate (pH 7.2), 7.5 mM $CaCl_2$, and 4 mM SC1982 prepared in DMSO-d_6] and mother liquor [40% 2-methyl-2,4-pentanediol, 0.1 M Tris (pH 8.0), and 7.5 mM $CaCl_2$]. ^{Ca}S100B–SC1475 crystals were grown in sitting drops consisting of a 0.75:0.75 μL protein solution [40 mg/mL S100B, 10 mM cacodylate (pH 7.2), 7.5 mM $CaCl_2$, and 4 mM SC1475 prepared in DMSO-d_6] and mother liquor [40% 2-methyl-2,4-pentanediol, 0.1 M Bis-Tris (pH 6.0), and 7.5 mM $CaCl_2$]. ^{Ca}S100B–SC124 crystals were grown in sitting drops consisting of a 0.75:0.75 μL protein solution [40 mg/mL S100B, 10 mM cacodylate (pH 7.2), 7.5 mM $CaCl_2$, and 4 mM SC124 prepared in DMSO-d_6] and mother liquor [40% 2-methyl-2,4-pentanediol, 0.1 M Hepes

dx.doi.org/10.1021/bi5005552 | *Biochemistry* 2014, 53, 6628–6640

Table 1. Statistics of Reflection Data and Structure Refinements[a]

	SC124	SC1475	SC1982	SBi4172	SBi4434
space group	*P*21	*P*21	*C*2221	*P*21	*P*21
unit cell dimensions (Å)	34.7, 56.5, 48.3	35.0, 58.1, 47.9	34.6, 90.0, 60.8	35.0, 57.1, 48.0	35.2, 56.3, 48.1
unit cell angles (deg)	90.0, 110.1, 90.0	90.0, 111.2, 90.0	90.0, 90.0, 90.0	90.0, 111.0, 90.0	90.0, 108.8, 90.0
resolution range (Å)	35.35−1.58	35.40−2.18	36.17−1.65	44.82−1.73	21.69−1.08
no. of reflections observed	83472 (9120)	30768 (4167)	55035 (7875)	55396 (8136)	244228 (12126)
no. of unique reflections	23617 (3115)	9152 (1259)	11752 (1673)	17118 (2517)	70592 (3504)
no. of reflections in the R_{free} set	1201	935	1173	869	2006
completeness (%)	97.8 (89.1)	96.7 (91.7)	99.9 (99.8)	92.6 (94.2)	92.2 (93.0)
redundancy	3.5 (2.9)	3.4 (3.3)	4.7 (4.7)	3.2 (3.2)	3.5 (3.5)
$\langle I/\sigma \rangle$	22.6 (3.5)	11.6 (2.3)	22.7 (2.6)	13.8 (2.4)	9.0 (3.0)
R_{sym}[b]	0.029 (0.325)	0.051 (0.461)	0.045 (0.613)	0.038 (0.452)	0.068 (0.351)
R_{crys}[c]	0.215	0.213	0.177	0.230	0.192
R_{free}[d]	0.253	0.251	0.214	0.268	0.211
no. of amino acids	179	180	90	179	181
no. of protein atoms	1445	1454	751	1446	1464
no. of hetero atoms	20	46	29	30	36
no. of waters	173	19	137	76	321
rmsd[e] for bond lengths (Å)	0.020	0.013	0.012	0.024	0.015
rmsd[e] for bond angles (deg)	1.056	1.304	1.231	1.372	1.133
mean *B* factor (Å^2)	28.92	48.73	20.67	39.00	14.91
protein atoms (Å^2)	27.69	48.00	18.61	38.74	13.62
hetero atoms (Å^2)	44.54	71.95	28.82	38.00	22.01
water atoms (Å^2)	37.36	48.65	30.21	44.32	25.09
Ramachandran outliers (%)	0.0	0.0	0.0	0.0	0.0
Ramachandran favored (%)	100.0	98.9	100.0	98.9	99.4

[a]The numbers in parentheses represent values from the highest-resolution shell (1.66−1.58 Å for SC124, 2.3−2.18 Å for SC1475, 1.74−1.65 Å for SC1982, 1.82−1.73 Å for SBi4172, and 1.10−1.08 Å for SBi4434). Atom counts do not include H. [b]$R_{sym} = \sum_h(\sum_j|I_{hj} - \langle I_h\rangle|/\sum I_{h,j})$, where h is the set of Miller indices, j is the set of observations of reflection h, and $\langle I_h\rangle$ is the mean intensity. [c]$R_{crys} = \sum_h||F_{o,h}| - |F_{c,h}||/\sum_h|F_{o,h}|$. [d]$R_{free}$ was calculated using a percentage of the complete data set excluded from refinement. [e]Deviations from ideal values.

(pH 7.0), and 7.5 mM $CaCl_2$]. The crystals were grown over a period of 1−14 days at 295 K. Crystals were flash-cooled directly from the crystallization drop.

Data Collection and Processing. Diffraction data for ^{Ca}S100B−SBi4172 crystals were collected at the Northeastern Collaborative Access Team (NE-CAT) 24ID-C beamline at the Advanced Photon Source (Argonne National Laboratory, Argonne, IL). Data were recorded at 100 K on a PILATUS detector and processed by NE-CAT's RAPD automated processing (https://rapd.nec.aps.anl.gov/rapd), which uses XDS[39] for integration and scaling. A 1.73 Å data set was collected at a wavelength of 0.97920 Å while the crystal was being oscillated by 1.0° each frame. The space group was determined to be *P*21.

Diffraction data for ^{Ca}S100B−SC124, ^{Ca}S100B−SBi4434, and ^{Ca}S100B−SC1982 crystals were collected remotely[40,41] at Stanford Synchrotron Radiation Lightsource (SSRL) beamline 7-1. Data were recorded at 100 K on an ADSC Q315 (315 mm × 315 mm) detector with collection strategies generated by BLU-ICE.[42] ^{Ca}S100B−SC124 and ^{Ca}S100B−SC1982 data sets were processed and integrated by AUTOXDS,[43] while S100B−SBi4434 data sets were processed and integrated by MOSFLM[44] within the CCP4 program suite.[45] A 1.58 Å ^{Ca}S100B−SC124 data set was collected at a wavelength of 1.1271 Å while the crystal was being oscillated by 0.6° each frame. The space group was determined to be *P*21. A 1.08 Å ^{Ca}S100B−SBi4434 data set was collected at a wavelength of 1.00 Å while the crystal was being oscillated by 0.35° each frame. The space group was determined to be *P*21. A 1.65 Å ^{Ca}S100B−SC1982 data set was collected at a wavelength of 1.1271 Å while the crystal was being oscillated 0.45° each frame. The space group was determined to be *C*2221.

Diffraction data for ^{Ca}S100B−SC1475 crystals were collected remotely[40,41] at Stanford Synchrotron Radiation Lightsource (SSRL) beamline 12-2. Data were recorded at 100 K on a PILATUS detector with collection strategies generated by BLU-ICE,[42] and processing and integration were performed by AUTOXDS.[43] A 2.18 Å data set was collected at a wavelength of 0.97950 Å while the crystal was being oscillated by 0.15° each frame. The space group was determined to be *P*21. Diffraction data statistics are summarized in Table 1.

Structure Determination and Refinement. To determine the structure of ^{Ca}S100B in complex with SBi*X*s, we performed molecular replacement (MR). A search model from a previous S100B structure [Protein Data Bank (PDB) entry 1MHO[46,47]] was generated by removing coordinates for ligands and water. Molecular replacement was conducted within the AUTOMR[48] function of the PHENIX[49] software suite. The models were finished by manual building within COOT.[50] The models were refined by the PHENIX.REFINE[51] function of the PHENIX[49] software suite. Ligands and waters were incorporated into the models by visual inspection of the $|F_o| - |F_c|$ omit maps. The structure refinement statistics are summarized in Table 1.

Cell-Based Assay with WM115 Malignant Melanoma Cells. The malignant melanoma cell line, WM115, was obtained from American Type Tissue Collection (ATCC) and cultured in minimum essential medium (Invitrogen) supplemented with 10% heat-inactivated fetal bovine serum (FBS) and 100 units/mL penicillin-streptomycin (PS). The cells were infected with SMARTvector 2.0 lentiviral particles

dx.doi.org/10.1021/bi5005552 | *Biochemistry* 2014, 53, 6628−6640

containing either nontargeting scrambled or anti-S100B shRNA according to manufacturer's recommendations (Thermo Scientific-Dharmacon). The following day, the medium containing lentivirus was removed, the cells were washed twice with PBS and trypsinized, and each well was expanded into a 24-well plate containing growth medium supplemented with puromycin (0.5 μg/mL). Upon confluence, the wells were trypsinized and single-cell diluted into 96-well plates. Positive clones with a reduction in the level of S100B protein expression were maintained in puromycin-containing medium.[52]

A cellular screen was then developed with these WM115 cell lines, and further test compounds were shown to bind S100B *in vitro*. In this cellular assay, the ability of SBi*X* molecules to inhibit the growth of WM115 melanoma cells infected with shRNA lentivirus (Dharmacon) targeting S100B ($shRNA^{S100B}$, i.e., low S100B) or a scrambled control ($shRNA^{scrambled}$, i.e., high S100B) was examined quantitatively. The methods used were similar to those used previously and included the use of a Biomek FX Laboratory Automation Workstation (Beckman-Coulter) equipped with a 96-channel pipetting head.[53] Specifically, 20 μL of MEM (Corning) supplemented with 10% fetal bovine serum, 0.5 μg/mL puromycin, and 1% Pen/Strep was added to each well of a 384-well, clear bottom, tissue culture plate (Corning) containing 600 cells per well such that growing uninhibited they reach 80% confluence in 5 days. After the cells had grown for 24 h at 37 °C in a 5% CO_2 humidity-controlled incubator, 20 μL of the compound was added directly to the cell culture medium, while control cultures received an equivalent amount of DMSO. After being incubated for an additional 4 days, the cells were lysed by transferring 20 μL of lysis buffer consisting of 1.8% Igepal with a 1:10000 dilution of SYBR Green I (10000×, Invitrogen) to each well. The plates were then returned to the incubator for 24 h. The fluorescence intensity was then read through the bottom of the plate using a PolarStar fluorescent plate reader (BMG) using 485 nm excitation and 520 nm emission filters. The SYBR Green fluorescence is used to measure total DNA that in turn correlates with the cell number as previously described.[54] The EC_{50} of each compound was determined using serial dilutions and performed in a minimum of three replicates. Hill curves of each replicate were generated using Origin Data Analysis Software.

To analyze changes in total p53 protein levels upon treatment with SC1982, WM115 cells were seeded in triplicate at a density of 70 × 10^5 cells in 60 mm dishes in 1× MEM (Cellgro) supplemented with 10% FBS, 100 units/mL PS, and 0.5 μg/mL puromycin and allowed to adhere overnight. The following day, the old medium was removed and new medium containing 5 μM SC1982 or DMSO was added. The cells were harvested 4 h post-treatment using cold 1× RIPA lysis buffer [0.5 M Tris-HCl (pH 7.4), 1.5 M NaCl, 2.5% deoxycholic acid, 10% Igepal, and 10 mM EDTA] and subjected to Western blotting.

Western blotting was performed using 30 μg of cell lysates loaded on a 12% sodium dodecyl sulfate−polyacrylamide gel electrophoresis gel (NuPage), which was subsequently transferred to PVDF membranes (Millipore) and reacted with p53 mouse monoclonal antibody (DO-1, Santa Cruz), mouse anti-S100B antibody (BD Biosciences), and mouse anti-GAPDH antibody at dilutions recommended by the manufacturers. The blots were then reacted with goat anti-mouse secondary antibodies (Kirkegaard & Perry Laboratories) and treated with Immobilon Western Chemiluminescent HRP Substrate (Millipore) at dilutions recommended by the manufacturer.

RESULTS

The binding of ^{Ca}S100B to p53 downregulates tumor suppressor activity in cancer cells such as malignant melanoma,[18,24] so a search for small molecule inhibitors that bind ^{Ca}S100B and prevent formation of the ^{Ca}S100B−p53 complex was undertaken. A fluorescence polarization competition assay (FPCA) was performed against the 1280-compound Library of Pharmacologically Active Compounds (*LOPAC1280*). Because of the location of Cys84 within the ^{Ca}S100B binding pocket (i.e., between sites 1 and 3), the focus of this investigation was a series of covalent complexes from this that were predicted to covalently bind at Cys84 of ^{Ca}S100B. SBi4172 is a structural analogue of the covalent modifier SC0844[35] and was thought to bind similarly. SC124, or disulfiram, is a known covalent modifier.[55] The chemical nature of SBi4434 suggests the possibility of adduct formation and is confirmed here. To gain additional opportunities for characterization of covalent adducts, compounds were also taken from a previously reported screen versus the 2000-compound Spectrum Collection.[35] The compounds characterized in this study include SC1982 and SC1475, which were reported in the previous study as being dependent on Cys84 for binding, but the formed covalent adducts were not investigated.[35] Cellular and biophysical characterization of these covalently bound inhibitors was explored, including their three-dimensional structures when bound to ^{Ca}S100B (Tables 1−4).

Table 2. Cellular Assays[a]

	high S100B EC_{50} (μM)		low S100B EC_{50} (μM)				
compound	mean	SD	mean	SD	*T*-test	ratio (∓)	*n*
SC124	0.06	0.06	0.23	0.38	0.321	3.57	6
SC1475	13.87	1.70	13.81	5.00	0.980	1.00	6
SC1982	5.05	1.13	8.95	2.68	0.001	1.77	8
SBi4172	2.07	1.29	3.11	1.43	0.127	1.50	9
SBi4434	FI		FI				

[a]Assays used WM115 melanoma cells transfected with $shRNA^{scrambled}$ (i.e., high S100B) or $shRNA^{S100B}$ (i.e., low S100B).

Table 3. Calculated rmsd's (angstroms) of Models from C$^{\alpha}$ Atoms of 1MHO[a]

^{Ca}S100B−SC124	0.382 (0.381)	0.435 (0.328)
^{Ca}S100B−SC1475	0.329 (0.258)	0.325(0.256)
^{Ca}S100B−SC1982	0.391 (0.279)	
^{Ca}S100B−SBi4172	0.518 (0.378)	0.546 (0.382)
^{Ca}S100B−SBi4434	0.310 (0.279)	0.319 (0.252)

[a]One or both modeled protein chains (when applicable) are compared to the single-protein chain within 1MHO. Numbers in parentheses are the calculated rmsd's of only globally conserved residues 1−84.

NMR Studies. Backbone resonance assignments were completed for each SBi*X*−S100B complex using standard multidimensional heteronuclear NMR data, and the chemical shift perturbations in ^{Ca}S100B (with or without the compound) were evaluated as described for other S100B inhibitors.[31,33−36] In general, the SBi*X* complexes studied here showed the largest perturbations within a well-defined binding pocket of ^{Ca}S100B comprising helices 3 and 4 and loop 2 (termed the "hinge"

dx.doi.org/10.1021/bi5005552 | *Biochemistry* 2014, 53, 6628−6640

Table 4. Measured Distortions of the Zinc Binding Site[a]

	His15	His25	His85	Glu89
SC1982	95.5°	19.1°	0.7 Å	1.9 Å
SBi4172	76.9°		1.4 Å	2.5 Å
SBi4434		28.1°	67.9°	1.5 Å
SC1475	68.2°		0.8 Å	1.3 Å
SC124	82.9°		1.0 Å	1.6 Å
SC0844[35]	38.3°	2.8 Å	157.7°	5.0 Å
SC0322[35]	31.2°	31.7°	49.1°	not applicable

[a]Shown are averaged movements of side chains in angstroms (directional movement of C^{γ}) or degrees (swing of $C^{\beta}-C^{\gamma}$). As Glu89 was not modeled in 1MHO, directional measurements are from the carbonyl carbon atom of Phe88.

region). These observations are consistent with the FPCA, which identified SBi*X*s that compete with TRTK12 peptide binding.

Chemical Shift Assignments. Titrations of compound into ^{Ca}S100B were monitored using $^{1}H-^{15}N$ HSQC NMR experiments, as previously described.[32−34] Because perturbations were not always easily tracked during the titration, a series of HNCA, HNCOCA, ^{15}N-edited NOESY-HSQC, and ^{15}N-HNH (HMQC-NOESY-HSQC) NMR experiments were collected at the end of each titration to unambiguously assign all the chemical shift values in the compound-bound state. The reaction products for five small molecules (SC124, SC1475, SC1982, SBi4172, and SBi4434) bound to ^{Ca}S100B were assessed by monitoring perturbations of backbone $^{1}H-^{15}N$ HSQC correlations after the compounds were added and fully reacted (Figure 2 and Figures S1−S5 of the Supporting Information).

In the presence of SC124, many of the $^{1}H-^{15}N$ HSQC correlations of ^{Ca}S100B were perturbed, with the most significant perturbations (≥mean ± SD) occurring for residues in loop 2 (His42) and helix 4 (Ser78, Thr81, Thr82, Ala83, Glu86, Phe87, and His90). Likewise, several other residues in loop 2 (Phe43, Leu44, Glu45, and Glu46) and helix 4 (Cys84, His85, and Glu89) either broadened and/or disappeared upon addition of SC124.

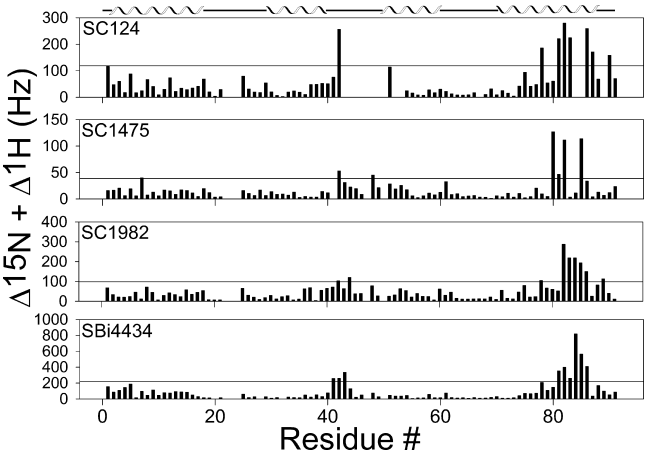

Figure 2. Assigned two-dimensional $^{1}H-^{15}N$ HSQC NMR spectra. The binding of five small molecules (SC124, SC1475, SC1982, SBi4172, and SBi4434) to ^{Ca}S100B was assessed by monitoring perturbations of backbone $^{1}H-^{15}N$ HSQC NMR experiments. Chemical shift perturbations in NMR spectra for ^{Ca}S100B in the presence of SBi4172 could not be measured as the compound caused ^{Ca}S100B to from soluble aggregates. The solid horizontal line is plotted at the mean perturbation (in hertz) plus one standard deviation for each data set.

Similarly, residues in loop 2 and helix 4 were perturbed for modifications via SC1982 (loop 2, His42 and Leu44; helix 4, Ser78, Thr82, Ala83, Cys84, His85, Glu86, and Glu89) and SBi4434 (loop 2, Ser41, His42, and Phe43; helix 4, Thr81, Thr82, Ala83, Cys84, His85, and Glu86). For SC1475, changes in loop 2 (His42 and Lys48), helix 4 (Val80, Thr81, Thr82, and His85), and helix 1 (Met7) were found in solution. These data are all consistent with the notion that SC124, SC1475, and SC1982 all react with Cys84 because loop 2 and helix 4 are in the proximity of each other in the crystallographic structures of ^{Ca}S100B and have been previously described to facilitate the binding of small molecules. For SBi4172, the chemical shift perturbations during the reaction could not be measured because the compound induced aggregation of ^{Ca}S100B (Figure S4 of the Supporting Information). To further characterize the structural impact of covalent modifications at Cys84 on ^{Ca}S100B, we next determined the structures of the S100B complexes with each compound by X-ray crystallography.

Crystallographic Studies. *Covalent Modifications at Cys84 Affect Target Binding of ^{Ca}S100B.* The structures of ^{Ca}S100B−inhibitor complexes (SC124, SC1475, SC1982, SBi4172, and SBi4434) are compared, each of which was confirmed to have the SBi*X* molecule covalently bound to Cys84 of ^{Ca}S100B (Figure 3). In all five of these structural models, each ^{Ca}S100B subunit consists of four helices (helix 1, E2−G19; helix 2, K28−L40; helix 3, E49−D61; helix 4, D69−F88), two small antiparallel β-strands, and a Ca^{2+} ion bound to both the typical and noncanonical EF-hand calcium binding domains. Likewise, the typical EF-hand is in the "open" Ca^{2+}-bound conformation, as is generally found in ^{Ca}S100B structures,[25] and the dimer interface is aligned as a symmetric X-type four-helix bundle comprising helices 1, 1′, 4, and 4′.[32,34−36,47] Comparison of these five structures to that of ^{Ca}S100B (PDB entry 1MHO[47]) with no drug target reveals a strong conservation of the global fold (Table 3); however, deviations in the positions of several side chains in the target binding site of ^{Ca}S100B were observed, as necessary, to accommodate the binding of various SBi*X* molecules. These include residues in helix 4 and/or loop 4 and in helix 1 (i.e., His15) in some cases, as described below (i.e., for the ^{Ca}S100B−SC124 complex). The specifics of each structure also provide details of potential synthetic strategies for engineering a single molecule that occupies all three persistent "pockets" within the S100B target binding site, so the individual structures and specific structural changes will be discussed in some detail.

^{Ca}S100B−SC124. The X-ray structure of a product resulting from mixing SC124 (disulfiram) with Ca^{2+}-bound S100B (^{Ca}S100B−SC124) was determined at 1.58 Å resolution (Figure 4). The asymmetric unit included two ^{Ca}S100B subunits (chains A and B) forming the biologically active form of dimeric ^{Ca}S100B. Residues Met0−Phe88 and Met0−Glu89 were modeled in chains A and B, respectively. In the final refined model (R_{crys} and R_{free} values of 0.215 and 0.253, respectively), all residues were in the favored (100%) regions of the Ramachandran plot with no outliers (Table 1). Each subunit of ^{Ca}S100B−SC124 was found to coordinate two calcium ions as is typical of S100 proteins,[38] and electron density was also clearly observed in the target binding sites for

dx.doi.org/10.1021/bi5005552 | *Biochemistry* 2014, 53, 6628−6640

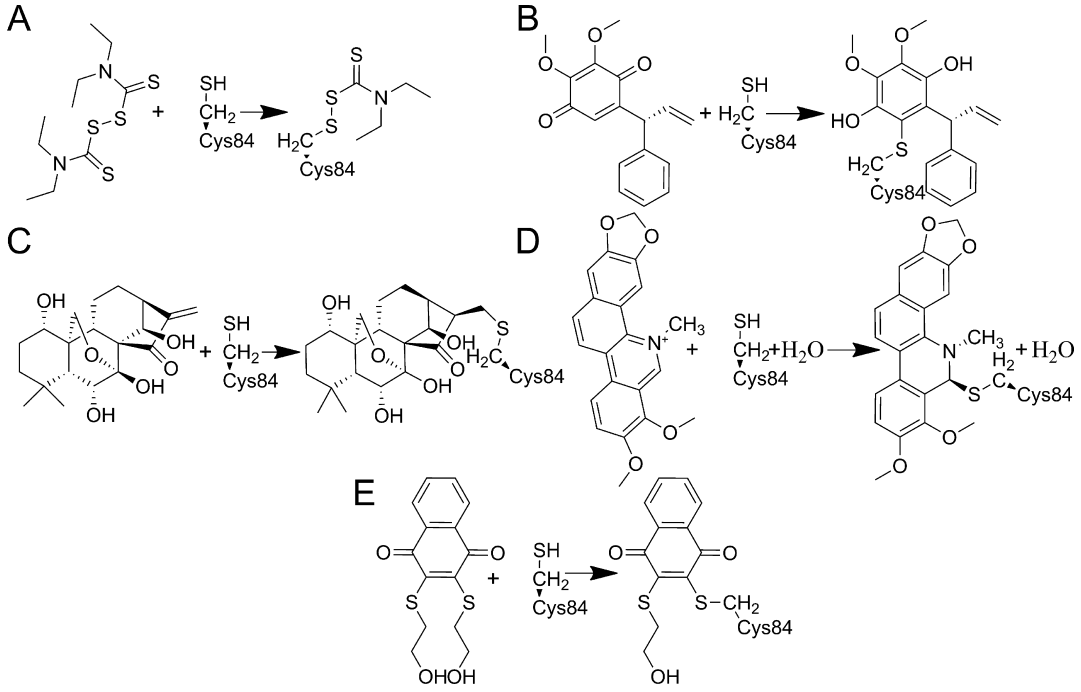

Figure 3. Chemical modification of Cys84 of ^{Ca}S100B. Shown are schematics that provide an overview of the chemical modification of Cys84 by compounds (A) SC124, (B) SC1475, (C) SC1982, (D) SBi4172, and (E) SBi4434.

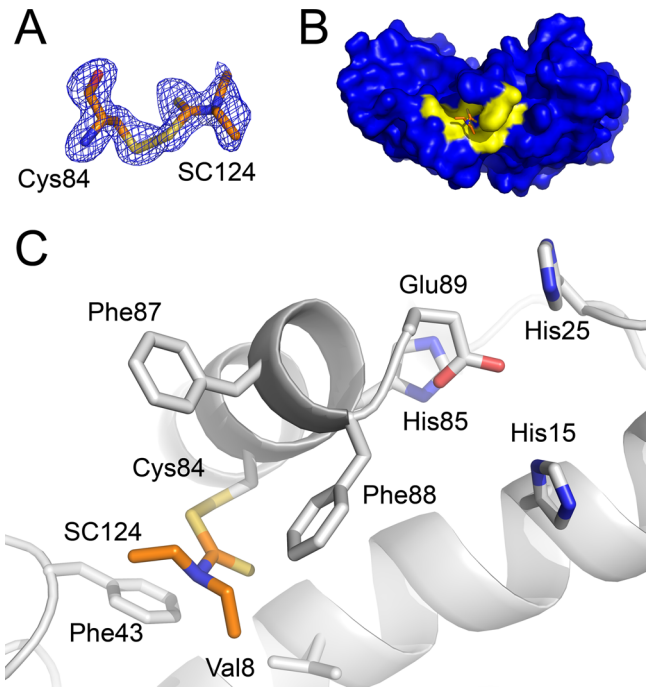

Figure 4. Crystallographic structure of the ^{Ca}S100B−SC124 complex. (A) Shown is an $|F_o| - |F_c|$ electron density omit map of SC124 covalently bound to Cys84 of ^{Ca}S100B with the map contoured at the 2.5σ level. (B) Dimeric ^{Ca}S100B is rendered in a surface diagram with residues within 4 Å of the SC124 colored yellow. SC124 is found within persistent binding site 2. (C) SC124 is situated within the hydrophobic pocket formed by Val8, Phe43, Phe87, and Phe88. SC124 makes no hydrogen bonds. The neighboring Zn^{2+} binding site composed of Glu89, His15, His25, and His85 is also rendered.

each subunit of ^{Ca}S100B as a result of nucleophilic attack of Cys84 by SC124 (Figures 3 and 4). The structure of the bound product was also consistent with what has been found previously with other protein adducts involving SC124[55] (Figure 3). Interestingly, though, the Cys84-bound SC124 adduct has somewhat different positions in each subunit of ^{Ca}S100B, and this was the first indication that this region, termed site 2, of ^{Ca}S100B can accommodate various orientations for small inhibitors. Curiously, the binding of SC124 causes the side chain of Glu89 in one subunit to occupy a pocket that can tightly coordinate a Zn^{2+} ion,[36,56,57] and as a result, His15 is reoriented. Note, in Zn^{2+}-bound structures of ^{Ca}S100B described elsewhere,[36,56,57] Zn^{2+} is coordinated by residues His15, His25, His85, and Glu89.

S100B−SC1475. The X-ray structure of a product resulting from mixing SC1475 (3,4-dimethoxydalbergione) with Ca^{2+}-bound S100B (^{Ca}S100B−SC1475) was determined at 2.18 Å resolution (Figure 5). The asymmetric unit included two ^{Ca}S100B subunits (chains X and A) of ^{Ca}S100B, and in both chains, residues Met0−Glu89 were modeled into the electron density. In the final refined structure (R_{crys} and R_{free} values of 0.213 and 0.251, respectively), all residues were in the most favored (98.9%) or allowed (1.1%) regions of the Ramachandran plot with no outliers (see Table 1). In each subunit, two Ca^{2+} ions, one SC1475 molecule, and 19 waters were resolved from the calculated electron density of the ^{Ca}S100B−SC1475 structure. It was also clear that SC1475 covalently modified ^{Ca}S100B via nucleophilic substitution of Cys84 into the benzoquinone moiety of the drug. Such a reaction is not uncommon, has been observed in toxic metabolites of acetaminophen, and results in the tautomerization of the moiety (Figure 3), as previously found.[58] Upon inspection, no hydrogen bonds were observed from residues of ^{Ca}S100B to SC1475, but the small molecule was situated in a hydrophobic pocket defined by residues in loop 2, termed the "hinge region" of S100B (Phe43) and helix 4 (Ile80, Ala83, Phe87, and Phe88). Specifically, the hydroquinone moiety of SC1475 stacks with Phe43, and the alkene moiety aligns favorably with the aromatic ring of Phe87. His15 is observed to swing outward

dx.doi.org/10.1021/bi5005552 | *Biochemistry* 2014, 53, 6628−6640

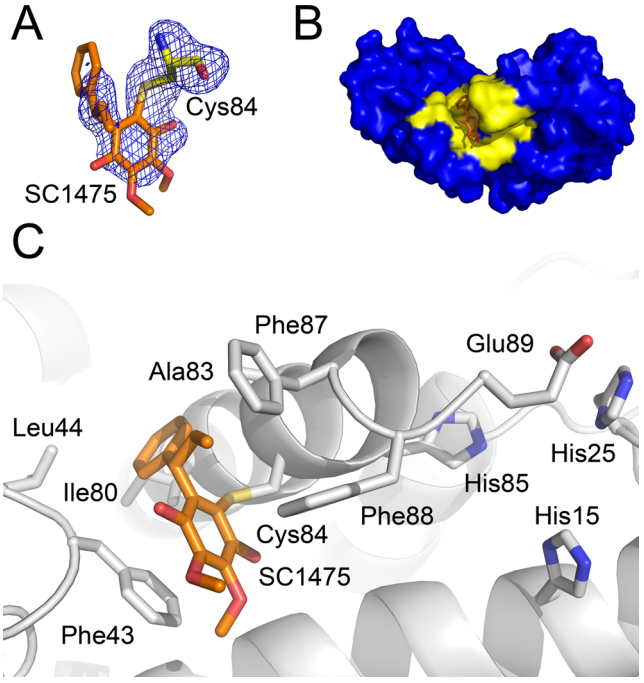

Figure 5. Crystallographic structure of the ^{Ca}S100B−SC1475 complex. (A) Shown is an $|F_o| - |F_c|$ electron density omit map of SC1475 covalently bound to Cys84 of ^{Ca}S100B with the map contoured at the 2.5σ level. (B) Dimeric ^{Ca}S100B is rendered in a surface diagram with residues within 4 Å of the SC1475 colored yellow. SC1475 is found within persistent binding site 2. (C) SC1475 is situated within the hydrophobic pocket formed by Phe43, Leu44, Ile80, Ala83, Phe87, and Phe88. SC1475 makes no hydrogen bonds. The neighboring Zn^{2+} binding site composed of Glu89, His15, His25, and His85 is also rendered.

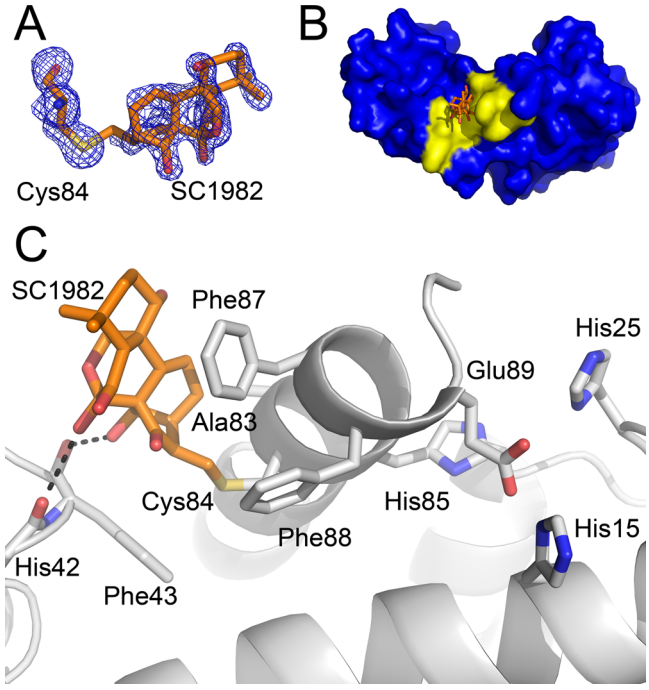

Figure 6. Crystallographic structure of the ^{Ca}S100B−SC1982 complex. (A) Shown is an $|F_o| - |F_c|$ electron density omit map of SC1982 covalently bound to Cys84 of ^{Ca}S100B with the map contoured at the 2.5σ level. (B) Dimeric ^{Ca}S100B is rendered in a surface diagram with residues within 4 Å of the SC1982 colored yellow. SC1982 is found within persistent binding site 2. (C) SC1982 is situated within the hydrophobic pocket formed by Phe43, Ala83, Phe87, and Phe88. SC1982 makes hydrogen bonds to the backbone carbonyls of His42 and Phe43. The neighboring Zn^{2+} binding site composed of Glu89, His15, His25, and His85 is also rendered.

from the Zn^{2+} binding site as observed in other ^{Ca}S100B−SBi*X* structures, and unlike ^{Ca}S100B complexes of SBi4172, SC124, and SC1982, Glu89 does not invade the Zn^{2+} binding site (*vide infra*).

^{Ca}S100B−SC1982. The X-ray structure of ^{Ca}S100B bound to SC1982 (Rubescensin A; ^{Ca}S100B−SC1982) was determined at 1.65 Å resolution (Figure 6). The asymmetric unit contained one ^{Ca}S100B subunit, and density for Met0−Glu91 could be readily modeled with the second subunit mapped on the basis of its location within the crystal symmetry. In the final refined model (R_{crys} and R_{free} values of 0.177 and 0.214, respectively), all residues were in the highly favored (100%) region of the Ramachandran plot with no outliers (Table 1). Each subunit of ^{Ca}S100B−SC1982 was found to coordinate two Ca^{2+} ions (one in each EF-hand), and one SC1982 molecule occupied each of the target protein binding sites via covalent modification (in the region termed site 2). Specifically, the alkene of SC1982 is reduced via Michael addition from the thiol of Cys84 from ^{Ca}S100B[59] (Figure 3). After covalent attachment, SC1982 makes two hydrogen bonds to the backbone carbonyls of loop 2 (His42 and Phe43) and forms several hydrophobic interactions with residues in the target binding pocket of ^{Ca}S100B, including those in loop 2 (Phe43) and helix 4 (Ile80, Phe87, and Phe88). His15 is once again observed to move outward from the Zn^{2+} binding site, and like the structures of ^{Ca}S100B−SC124 and ^{Ca}S100B−SBi4172, the covalent binding of SC1982 causes the side chain of Glu89 to intrude into a region of the protein, which can bind Zn^{2+}, and causes the side chain of His15 to rotate away fairly drastically.

Electron density for a highly coordinated atom that is too dense to be water was identified. As calcium is prevalent in the system and because of the identity of the contributors in the coordination (Asp63, Asp69, and six water molecules), a third calcium ion was modeled into this density (confirmed by anomalous difference maps).

^{Ca}S100B−SBi4172. The X-ray structure of chelerythrine-bound ^{Ca}S100B, ^{Ca}S100B−SBi4172, was determined at 1.73 Å resolution (Figure 7). The asymmetric unit in the drug complex included two S100B subunits (chains A and B) forming the biologically active dimeric form of ^{Ca}S100B. In chain A, residues Met0−Glu89 were modeled into the electron density, and in chain B, only Ser1−Glu89 could be resolved. Each subunit of the ^{Ca}S100B−SBi4172 complex coordinated two Ca^{2+} ions; however, only one molecule of SBi4172 could be observed and was located in the model for chain B. Sparse density was observed in the analogous binding pocket of chain A, but it was not sufficiently well defined for accurate modeling of the SBi4172 inhibitor. A more detailed analysis of chain A showed that a lack of density in the second subunit likely occurred as a result of spatial restraints imposed by the crystal packing. In the final refined model (R_{crys} and R_{free} values of 0.230 and 0.268, respectively), all residues in both subunits were in the favored (98.9%) or allowed regions (1.1%) of the Ramachandran plot with no outliers (Table 1). As clearly defined by the calculated electron density maps, SBi4172 was found to react with Cys84 via hydration of a double bond of SBi4172[60] (Figure 3). Once SBi4172 was covalently bound, a dioxole oxygen atom of SBi4172 was found to make water-bridged interactions with the

dx.doi.org/10.1021/bi5005552 | *Biochemistry* 2014, 53, 6628−6640

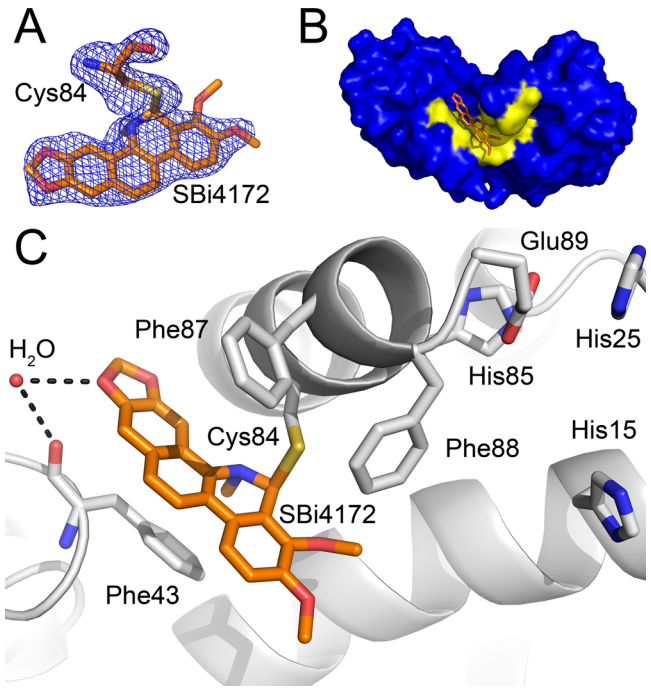

Figure 7. Crystallographic structure of the ^{Ca}S100B−SBi4172 complex. (A) Shown is an $|F_o| - |F_c|$ electron density omit map of SBi4172 covalently bound to Cys84 of ^{Ca}S100B with the map contoured at the 2.5σ level. (B) Dimeric ^{Ca}S100B is rendered in a surface diagram with residues within 4 Å of the SBi4172 colored yellow. SBi4172 is found within persistent binding site 2. (C) SBi4172 is situated within the hydrophobic pocket formed by Phe43, Phe87, and Phe88. SBi4172 makes a water-bridged interaction with the backbone carbonyl of Phe43. The neighboring Zn^{2+} binding site composed of Glu89, His15, His25, and His85 is also rendered.

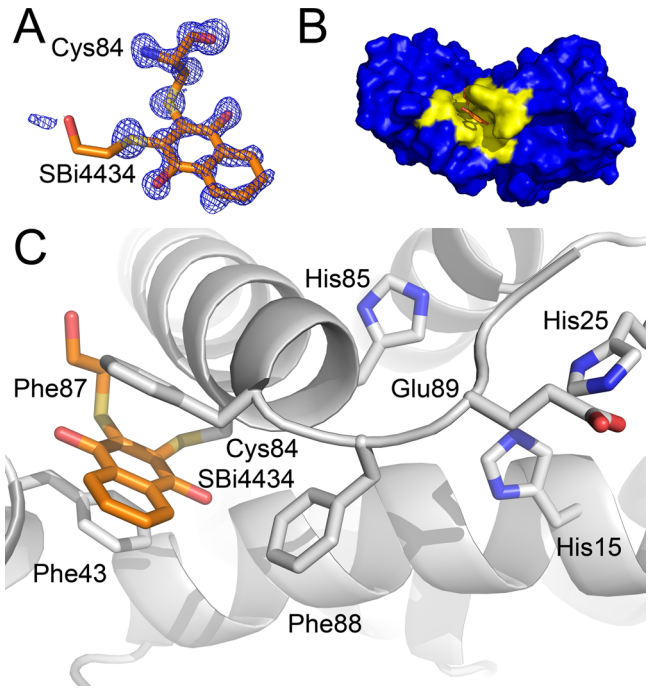

Figure 8. Crystallographic structure of the ^{Ca}S100B−SBi4434 complex. (A) Shown is an $|F_o| - |F_c|$ electron density omit map of SBi4434 covalently bound to Cys84 of ^{Ca}S100B with the map contoured at the 2.5σ level. (B) Dimeric ^{Ca}S100B is rendered in a surface diagram with residues within 4 Å of the SBi4434 colored yellow. SBi4434 is found within persistent binding site 2. (C) SBi4434 is situated within the hydrophobic pocket formed by Phe43, Phe87, and Phe88. SBi4434 makes no hydrogen bonds. The neighboring Zn^{2+} binding site composed of Glu89, His15, His25, and His85 is also rendered.

backbone carbonyl of Phe43. Otherwise, SBi4172 was situated in a hydrophobic pocket composed of side chains within loop 2 (Phe43), helix 4 (Ile80, Ala83, Phe87, and Phe88), and helix 1′ (Val7, Val8, and Ile11). Like the earlier inhibitor-bound ^{Ca}S100B complexes, the side chain moiety of His15 was found to move out of the established Zn^{2+} binding site of ^{Ca}S100B.

^{Ca}S100B−SBi4434. The X-ray structure of SBi4434 {2,3-bis[(2-hydroxyethyl)thio]-1,4-naphthoquinone} bound to ^{Ca}S100B (^{Ca}S100B−SBi4434) was determined at 1.08 Å resolution (Figure 8). The asymmetric unit included two S100B subunits (chains A and X) forming the biologically active dimeric form of S100B. In chain A, residues Met0−Glu91were modeled while only residues Met0−Phe88 of chain X could be resolved. Each subunit in the ^{Ca}S100B−SBi4434 structure bound two calcium ions and a SBi4434 molecule. In the final refined model (R_{crys} and R_{free} values of 0.192 and 0.211, respectively), all residues were in the favored (99.4%) or allowed regions (0.6%) of the Ramachandran plot with no outliers (Table 1). Sole among the structures described here, the high resolution of the diffraction data produced by the ^{Ca}S100B−SBi4434 crystal allowed for the inclusion of riding hydrogen atoms in this particular model. As clearly defined by the calculated electron density maps, SBi4434 covalently modifies ^{Ca}S100B at Cys84. As seen, the thiol of Cys84 substitutes for one of the thioglycol moieties of SBi4434 (Figure 3). The second thioglycol moiety is allowed much conformational flexibility as evidenced by the sparse electron density for these atoms as well as the alternative conformations of the moiety modeled in the two inhibitor molecules. The compound does not make any hydrogen bonds with the protein but is nestled in a hydrophobic pocket formed by loop 2 and helix 4 with the aromatic rings of SBi4434 stacked between the side chains of Phe43 and Phe87. In this model, His85 swings out of the Zn^{2+} binding site.

Coordinates and structure factors have been deposited in the Protein Data Bank as entries 4PE1 for ^{Ca}S100B−SC124, 4PE4 for ^{Ca}S100B−SC1475, 4PE7 for ^{Ca}S100B−SC1982, 4PDZ for ^{Ca}S100B−SBi4172, and 4PE0 for ^{Ca}S100B−SBi4434.

Cell-Based Assay. To determine whether covalent modification of Cys84 affects cell proliferation in malignant melanoma, its effect on the growth of WM115 malignant melanoma cells, which express elevated levels of the S100B protein, was measured as described previously.[53] Briefly, proliferation of WM115 cells stably transfected with either shRNA^{scrambled} (i.e., high S100B) or shRNA^{S100B} (i.e., low S100B) was evaluated in triplicate following a 4 day incubation in the absence or presence of each compound at varying concentrations (Table 2). For each titration, knockdown of the S100B protein was confirmed by Western blot analysis (3-fold decrease; n = 4) (Figure 9), and EC_{50} values were determined using the average of three or more titrations. With SC1475 as an exception (ratio of 1.00), it was found that lower concentrations of SC124, SC1982, and SBi4172 were needed to inhibit cell growth with the shRNA^{scrambled} versus the shRNA^{S100B} knockdown WM115 cells (1.50 < ratio < 3.57). This is consistent with the compounds having specificity

dx.doi.org/10.1021/bi5005552 | *Biochemistry* 2014, 53, 6628−6640

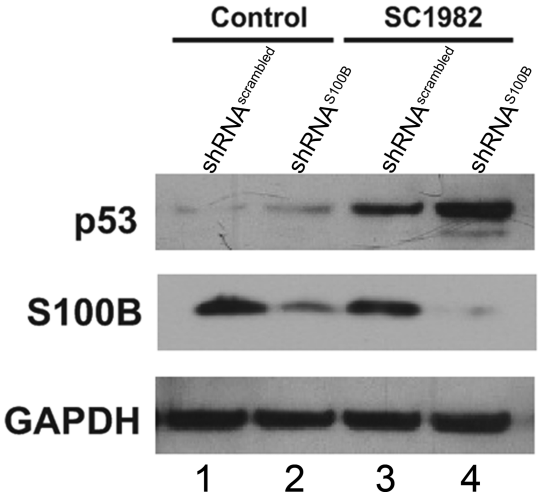

Figure 9. Westen blot analysis. The control without drug was treated with the same DMSO concentration (0.01%). The addition of SC1982 did not affect the protein levels of S100B in the shRNA^{scrambled} or shRNA^{S100B} cell lines. However, both shRNA^{scrambled} and shRNA^{S100B} cell lines had a measurable gain in total p53 protein levels in the presence of SC1982. This result along with an observation of S100B expression-dependent growth inhibition suggests that SC1982 displays an on-target effect of S100B inhibition with subsequent p53 restoration.

toward S100B-containing cells; however, only titrations with SC1982 were shown to be S100B-selective (1.77-fold) with a statistically significant *t*-test ($p = 0.001$; $n = 8$). Consistent with this result, p53 levels were 2-fold higher ($n = 4$) in the presence than in the absence of SC1982 (in Figure 9, compare lanes 1 and 3 and lanes 2 and 4, respectively). This result along with an observation of S100B expression-dependent growth inhibition suggests that SC1982 displays an on-target effect of S100B inhibition with subsequent p53 restoration. The last compound, SBi4434, showed fluorescence interference with the SYBR Green dye, so it was excluded from further evaluation.

DISCUSSION

Malignant melanoma is the fifth and seventh most common cancer among men and women,[61] respectively, so the discovery of novel therapeutics for its treatment remains a high priority. Elevated S100B is a prognostic indicator for assessing disease progression, disease recurrence, and metastatic potential in patients with MM.[62−68] It is also established that S100B not only is a clinical marker but also binds to and negatively regulates p53 at the protein level.[18,19] While the p53 tumor suppressor protein is mutated in many human cancers,[69] it is typically wild-type (wt, >90%) in MM,[26,27] so restoring p53 protein by inhibiting S100B represents a novel therapeutic strategy for treating MM. While low-molecular weight compounds that block the p53 binding site on S100B and inhibit formation of the S100B−p53 complex exist, improving their affinity, efficacy, and specificity remains a priority. Thus, S100B represents a new cancer target, and improved SBi*X*s should provide novel therapeutic(s) for treating MM by restoring active p53 protein.[27]

Structure−function characterizations of five novel inhibitors of the ^{Ca}S100B−p53 interaction are presented here. Of the five compounds, SC1982 has the most significant hydrogen bonding network within the ^{Ca}S100B binding pocket, and interestingly, it demonstrated the highest level of target specific activity in the WM115 cellular assay. Note that despite the relatively low EC_{50} of SC124, expectations should be tempered when considering this compound. SC124 is small with a scaffold lacking complexity. It forms no hydrogen bonds with the target protein and lacks even a consistent binding pose within the two monomers of S100B. These details leave little potential for SC124 as a therapeutic that would not be sequestered elsewhere within the cell, and unsurprisingly, it lacks statistically significant S100B expression-dependent growth inhibition.

Such target specific effects are important when considering the relationship between off-target effects and toxicity. This is particularly important when considering the therapeutic application of covalent modifiers because their off-target effects are not uncommon and are often severe. One successful example of a drug linked to the protein via Michael addition is Afatinib, which is used in the treatment of metastatic non-small cell lung carcinoma (NSCLC).[70,71] The target specific effect of SC1982 (Figure 9 and Table 2) is reassuring and warrants further investigation as a chemical scaffold for engineering novel SBi*X* molecules. In fact, SC1982 and each compound presented here offer a new chemical scaffold for continued SAR studies for improving affinity and specificity.

These structures can be used for guiding the design of new inhibitors using multiple approaches. The most straightforward of these is via "tethering" new functional moieties onto the existing covalently bound compound(s) and keeping the covalent bond in place.[72] A second strategy is to develop quickly reversible covalent modifications, as described previously,[73] for the inclusion of an α-cyanoacrylamide functionality. This modification increases the intrinsic reactivity of an olefin and eliminates the formation of irreversible adducts. Such an approach could enhance the bioavailability and selectivity of the inhibitory compound. For Cys84 of ^{Ca}S100B, such a cyanoacrylamide (or cyanoacrylate) would react with cysteine thiols under physiological conditions in an energetically favorable manner and become rapidly reversible, including having off rates on the subsecond to second time scales.[71] In this situation, the level of off-site targeting is significantly reduced, and the covalent nature of the adduct for the target of interest is long-lived, as needed for therapeutic efficacy.

A third approach to obtaining high-affinity, high-specificity S100B inhibitors with these data is to engineer compounds that make use of all three persistent pockets in the p53 binding site. In this regard, the inhibitors presented here are particularly important because they are located within the persistent binding pocket termed "site 2". Therefore, regardless of whether these inhibitors are covalently bound, they provide exquisite detail for how to connect chemical moieties in sites 1 and 3. Therefore, the inhibitors presented here can be considered in combination with chemical functionalities described in previous structural studies of other SBi*X*s[33−36] to produce a ligand capable of binding all three persistent binding sites simultaneously. The simultaneous occupation of sites 1 and 2 will be of interest first because "site 3" binders within ^{Ca}S100B have been thoroughly described elsewhere.

Although the mechanisms involved in adduct formation may differ between compounds, SC124, SC1475, SC1982, SBi4172, and SBi4434 (as well as for SC0844 and SC322[35] studied previously), together these compounds comprise a subset of S100B inhibitors that impact the conformational state of ^{Ca}S100B in a similar manner. In particular, an adduct added to

dx.doi.org/10.1021/bi5005552 | *Biochemistry* 2014, 53, 6628−6640

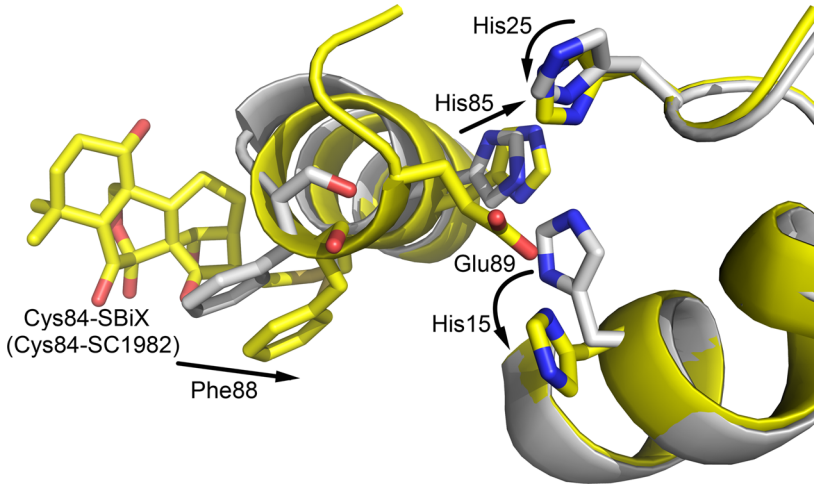

Figure 10. Distortion of the zinc binding site is a hallmark of the S100B covalent inhibitor family. Shown are ribbon diagrams of ^{Ca}S100B in the presence (yellow) and absence (gray) of a covalent modifier (SC1982) with residues and ligands of interest shown as sticks. The covalent modifier family of SBi*X*s is hallmarked by perturbation in the conformational state of the residues forming the Zn^{2+} binding site (His15, His25, His85, and Glu89). Commonly, Glu89 is seen intruding on the Zn^{2+} with a subsequent displacement of a histidine side chain.

Cys84 clashes with side chains on helix 4 and thereby rotates a Zn^{2+} binding residue, Glu89, into a new location. As a result, residues comprising the Zn^{2+} binding site (His15, His25, His85, and Glu89) are subsequently reordered. Although the particulars of this effect on the Zn^{2+} binding site may be unique to an individual compound and may or may not have an effect on S100B activities, the covalent modifier family of SBi*X*s described here is "hallmarked" by this common structural perturbation (Figure 10). Table 4 lists the effect through measurements of directional movements of atoms and torsions of residue side chains. The most disruptive feature of this conformational change is an intrusion of Glu89 into the Zn^{2+} site with a subsequent exit of one of the localized histidine side chains. Further investigation may prove this to be a meaningful observation because the oxidation of Cys84 has functional implications with regard to the regulation of S100B by redox.[74] The inhibitory properties of these compounds may in part be attributed to the manipulation of this natural regulatory Zn^{2+} binding feature of S100B and are very likely functionally important.

Although we have demonstrated a restoration in p53 levels alongside the inhibition of S100B, it must be noted that within WM115 malignant melanoma cells, S100B has been associated with factors other than p53. For instance, S100B was found to enhance cell viability and modulate MAPK signaling by binding directly to the p90 ribosomal S6 kinase (RSK). The formation of this complex blocks ERK-dependent phosphorylation of RSK and sequesters RSK into the cytosol, preventing it from acting on nuclear targets. Thus, S100B has been shown to increase the level of cell survival in malignant melanoma by contributing to abnormal ERK/RSK signaling.[52] Also, a target of S100B is the receptor for advanced glycation end products (RAGE). RAGE is upregulated in late metastatic stages of samples from melanoma patients. The overexpression of RAGE is associated with mesenchymal-like morphologies in WM115 cells and results in greater migration abilities and reduced proliferation properties. This supports a role of RAGE in the metastatic switch of melanoma cells. Interestingly, overexpression of RAGE results in the increased level of expression of S100B and lower levels of p53, ERK1/2, cyclin E, and NF-κB.[75]

■ ASSOCIATED CONTENT

Supporting Information

Figures S1−S5 show overlaid two-dimensional $^{1}H-^{15}N$ HSQC spectra of ^{Ca}S100B and ^{Ca}S100B−SBi*X* complexes. This material is available free of charge via the Internet at http://pubs.acs.org.

■ AUTHOR INFORMATION

Corresponding Author

*University of Maryland School of Medicine, Department of Biochemistry and Molecular Biology, Biomedical Research Facility, Rm. 439, 108 N. Greene St., Baltimore, MD 21201. E-mail: dweber@som.umaryland.edu. Phone: (410) 706-4354. Fax: (410) 706-0438.

Funding

This work was supported by grants from the National Institutes of Health (NIH) (GM58888 and CA107331) to D.J.W. The training of M.C.C. is supported by an NIH T32 grant (CA154274). Work performed at synchrotron facilities was supported by NIH Grants P41GM103403 (D.B.N., NE-CAT) and P41GM103393 (SSRL).

Notes

The authors declare no competing financial interest.

■ ACKNOWLEDGMENTS

Research conducted at the Advanced Photon Source on the Northeastern Collaborative Access Team beamlines is supported by the National Institutes of Health, National Institute of General Medical Sciences. Use of the Advanced Photon Source, an Office of Science User Facility operated for the U.S. Department of Energy (DOE) Office of Science by Argonne National Laboratory, was supported by the U.S. DOE. Use of the Stanford Synchrotron Radiation Lightsource, SLAC National Accelerator Laboratory, is supported by the U.S. DOE, Office of Science and Office of Basic Energy. The SSRL Structural Molecular Biology Program is supported by the DOE Office of Biological and Environmental Research and by the National Institutes of Health, National Institute of General Medical Sciences.

■ ABBREVIATIONS

MM, malignant melanoma; SBi*X*, S100B inhibitor where *X* is a number; ^{Ca}S100B, calcium-bound S100B; NMR, nuclear magnetic resonance; HSQC, heteronuclear single-quantum coherence; rmsd, root-mean-square deviation; SD, standard deviation.

■ REFERENCES

(1) Kwong, L. N., and Davies, M. A. (2014) Targeted therapy for melanoma: Rational combinatorial approaches. *Oncogene 33*, 1−9.

(2) Topalian, S. L., Hodi, F. S., Brahmer, J. R., Gettinger, S. N., Smith, D. C., McDermott, D. F., Powderly, J. D., Carvajal, R. D., Sosman, J. A., Atkins, M. B., Leming, P. D., Spigel, D. R., Antonia, S. J., Horn, L., Drake, C. G., Pardoll, D. M., Chen, L., Sharfman, W. H., Anders, R. A., Taube, J. M., McMiller, T. L., Xu, H., Korman, A. J., Jure-Kunkel, M., Agrawal, S., McDonald, D., Kollia, G. D., Gupta, A., Wigginton, J. M., and Sznol, M. (2012) Safety, activity, and immune correlates of anti-PD-1 antibody in cancer. *N. Engl. J. Med. 366*, 2443−2454.

(3) Bollag, G., Hirth, P., Tsai, J., Zhang, J., Ibrahim, P. N., Cho, H., Spevak, W., Zhang, C., Zhang, Y., Habets, G., Burton, E. A., Wong, B., Tsang, G., West, B. L., Powell, B., Shellooe, R., Marimuthu, A., Nguyen, H., Zhang, K. Y., Artis, D. R., Schlessinger, J., Su, F., Higgins, B., Iyer, R., D'Andrea, K., Koehler, A., Stumm, M., Lin, P. S., Lee, R. J., Grippo, J., Puzanov, I., Kim, K. B., Ribas, A., McArthur, G. A., Sosman, J. A., Chapman, P. B., Flaherty, K. T., Xu, X., Nathanson, K. L., and Nolop, K. (2010) Clinical efficacy of a RAF inhibitor needs broad target blockade in BRAF-mutant melanoma. *Nature 467*, 596−599.

(4) Flaherty, K. T., Puzanov, I., Kim, K. B., Ribas, A., McArthur, G. A., Sosman, J. A., O'Dwyer, P. J., Lee, R. J., Grippo, J. F., Nolop, K., and Chapman, P. B. (2010) Inhibition of mutated, activated BRAF in metastatic melanoma. *N. Engl. J. Med. 363*, 809−819.

(5) Espinosa, E., Grob, J. J., Dummer, R., Rutkowski, P., Robert, C., Gogas, H., Kefford, R., Eggermont, A. M., Martin Algarra, S., Hauschild, A., and Schadendorf, D. (2014) Treatment Algorithms in Stage IV Melanoma. *American Journal of Therapeutics*, DOI: 10.1097/MJT.0b013e31829e885c.

(6) Gogas, H., Abali, H., Ascierto, P. A., Demidov, L., Pehamberger, H., Robert, C., Schachter, J., Eggermont, A. M., Hauschild, A., and Espinosa, E. (2013) Who Benefits Most From Adjuvant Interferon Treatment for Melanoma? *American Journal of Therapeutics*, DOI: 10.1097/MJT.0b013e31829e883d.

(7) Jang, S., and Atkins, M. B. (2013) Which drug, and when, for patients with BRAF-mutant melanoma? *Lancet Oncol. 14*, e60−e69.

(8) Marcus, D. M., Lowe, M., Khan, M. K., Lawson, D. H., Crocker, I. R., Shelton, J. W., Melton, A., Maynard, N., Delman, K. A., Carlson, G. W., and Rizzo, M. (2013) Prognostic Factors for Overall Survival After Radiosurgery for Brain Metastases From Melanoma. *Am. J. Clin. Oncol.*, DOI: 10.1097/COC.0b013e318280d7be.

(9) Kashani-Sabet, M. (2014) Molecular markers in melanoma. *Br. J. Dermatol. 170*, 31−35.

(10) Riechers, A., and Bosserhoff, A. K. (2014) Melanoma inhibitory activity in melanoma diagnostics and therapy: A small protein is looming large. *Exp. Dermatol. 23*, 12−14.

(11) El Hajj, P., Journe, F., Wiedig, M., Laios, I., Sales, F., Galibert, M. D., Van Kempen, L. C., Spatz, A., Badran, B., Larsimont, D., Awada, A., and Ghanem, G. (2013) Tyrosinase-related protein 1 mRNA expression in lymph node metastases predicts overall survival in high-risk melanoma patients. *Br. J. Cancer 108*, 1641−1647.

(12) Henry, L., Fabre, C., Guiraud, I., Bastide, S., Fabbro-Peray, P., Martinez, J., Lavabre-Bertrand, T., Meunier, L., and Stoebner, P. E. (2013) Clinical use of p-proteasome in discriminating metastatic melanoma patients: Comparative study with LDH, MIA and S100B protein. *Int. J. Cancer 133*, 142−148.

(13) Wieder, H. A., Tekin, G., Rosenbaum-Krumme, S., Klode, J., Altenbernd, J., Bockisch, A., and Nagarajah, J. (2013) 18FDG-PET to assess recurrence and long term survival in patients with malignant melanoma. *Nuklearmedizin 52*, 198−203.

(14) Schiltz, P. M., Dillman, R. O., Korse, C. M., Cubellis, J. M., Lee, G. J., and De Gast, G. C. (2008) Lack of elevation of serum S100B in patients with metastatic melanoma as a predictor of outcome after induction with an autologous vaccine of proliferating tumor cells and dendritic cells. *Cancer Biother. Radiopharm. 23*, 214−221.

(15) O'Rourke, M. G., Johnson, M., Lanagan, C., See, J., Yang, J., Bell, J. R., Slater, G. J., Kerr, B. M., Crowe, B., Purdie, D. M., Elliott, S. L., Ellem, K. A., and Schmidt, C. W. (2003) Durable complete clinical responses in a phase I/II trial using an autologous melanoma cell/dendritic cell vaccine. *Cancer Immunol. Immunother. 52*, 387−395.

(16) Hartman, K. G., McKnight, L. E., Liriano, M. A., and Weber, D. J. (2013) The evolution of S100B inhibitors for the treatment of malignant melanoma. *Future Med. Chem. 5*, 97−109.

(17) Lin, J., Yang, Q., Wilder, P. T., Carrier, F., and Weber, D. J. (2010) The calcium-binding protein S100B down-regulates p53 and apoptosis in malignant melanoma. *J. Biol. Chem. 285*, 27487−27498.

(18) Lin, J., Yang, Q., Yan, Z., Markowitz, J., Wilder, P. T., Carrier, F., and Weber, D. J. (2004) Inhibiting S100B restores p53 levels in primary malignant melanoma cancer cells. *J. Biol. Chem. 279*, 34071−34077.

(19) Baudier, J., Delphin, C., Grunwald, D., Khochbin, S., and Lawrence, J. J. (1992) Characterization of the tumor suppressor protein p53 as a protein kinase C substrate and a S100b-binding protein. *Proc. Natl. Acad. Sci. U.S.A. 89*, 11627−11631.

(20) Rustandi, R. R., Baldisseri, D. M., Drohat, A. C., and Weber, D. J. (1999) Structural changes in the C-terminus of Ca^{2+}-bound rat S100B ($\beta\beta$) upon binding to a peptide derived from the C-terminal regulatory domain of p53. *Protein Sci. 8*, 1743−1751.

(21) Rustandi, R. R., Baldisseri, D. M., and Weber, D. J. (2000) Structure of the negative regulatory domain of p53 bound to S100B($\beta\beta$). *Nat. Struct. Biol. 7*, 570−574.

(22) Rustandi, R. R., Drohat, A. C., Baldisseri, D. M., Wilder, P. T., and Weber, D. J. (1998) The Ca^{2+}-dependent interaction of S100B($\beta\beta$) with a peptide derived from p53. *Biochemistry 37*, 1951−1960.

(23) Wilder, P. T., Rustandi, R. R., Drohat, A. C., and Weber, D. J. (1998) S100B($\beta\beta$) inhibits the protein kinase C-dependent phosphorylation of a peptide derived from p53 in a Ca^{2+}-dependent manner. *Protein Sci. 7*, 794−798.

(24) Lin, J., Blake, M., Tang, C., Zimmer, D., Rustandi, R. R., Weber, D. J., and Carrier, F. (2001) Inhibition of p53 transcriptional activity by the S100B calcium-binding protein. *J. Biol. Chem. 276*, 35037−35041.

(25) Weber, D. J., Rustandi, R. R., Carrier, F., and Zimmer, D. B. (2000) Interaction of dimeric S100B($\beta\beta$) with the tumor suppressor protein: A model for Ca-dependent S100-target protein interactions. In *The molecular basis of calcium action in biology and medicine* (Pochet, R., Ed.) pp 469−487, Kluwer Academic Publishers, Dordrecht, The Netherlands.

(26) Hussein, M. R., Haemel, A. K., and Wood, G. S. (2003) p53-related pathways and the molecular pathogenesis of melanoma. *Eur. J. Cancer Prev. 12*, 93−100.

(27) Brown, C. J., Lain, S., Verma, C. S., Fersht, A. R., and Lane, D. P. (2009) Awakening guardian angels: Drugging the p53 pathway. *Nat. Rev. Cancer 9*, 862−873.

(28) Smith, J., Stewart, B. J., Glaysher, S., Peregrin, K., Knight, L. A., Weber, D. J., and Cree, I. A. (2010) The effect of pentamidine on melanoma ex vivo. *Anticancer Drugs 21*, 181−185.

(29) Zimmer, D. B., Lapidus, R. G., and Weber, D. J. (2013) In vivo screening of S100B inhibitors for melanoma therapy. *Methods Mol. Biol. 963*, 303−317.

(30) Jochemsen, A. G. (2014) Reactivation of p53 as therapeutic intervention for malignant melanoma. *Curr. Opin. Oncol. 26*, 114−119.

(31) Markowitz, J., Chen, I., Gitti, R., Baldisseri, D. M., Pan, Y., Udan, R., Carrier, F., MacKerell, A. D., Jr., and Weber, D. J. (2004) Identification and characterization of small molecule inhibitors of the calcium-dependent S100B-p53 tumor suppressor interaction. *J. Med. Chem. 47*, 5085−5093.

(32) Charpentier, T. H., Thompson, L. E., Liriano, M. A., Varney, K. M., Wilder, P. T., Pozharski, E., Toth, E. A., and Weber, D. J. (2010) The effects of CapZ peptide (TRTK-12) binding to S100B-Ca^{2+} as examined by NMR and X-ray crystallography. *J. Mol. Biol. 396*, 1227−1243.
(33) Charpentier, T. H., Wilder, P. T., Liriano, M. A., Varney, K. M., Zhong, S., Coop, A., Pozharski, E., MacKerell, A. D., Jr., Toth, E. A., and Weber, D. J. (2009) Small molecules bound to unique sites in the target protein binding cleft of calcium-bound S100B as characterized by nuclear magnetic resonance and X-ray crystallography. *Biochemistry 48*, 6202−6212.
(34) McKnight, L. E., Raman, E. P., Bezawada, P., Kudrimoti, S., Wilder, P. T., Hartman, K. G., Godoy-Ruiz, R., Toth, E. A., Coop, A., Mackerell, A. D., Jr., and Weber, D. J. (2012) Structure-Based Discovery of a Novel Pentamidine-Related Inhibitor of the Calcium-Binding Protein S100B. *ACS Med. Chem. Lett. 3*, 975−979.
(35) Wilder, P. T., Charpentier, T. H., Liriano, M. A., Gianni, K., Varney, K. M., Pozharski, E., Coop, A., Toth, E. A., Mackerell, A. D., and Weber, D. J. (2010) In vitro screening and structural characterization of inhibitors of the S100B-p53 interaction. *Int. J. High Throughput Screening 2010*, 109−126.
(36) Charpentier, T. H., Wilder, P. T., Liriano, M. A., Varney, K. M., Pozharski, E., MacKerell, A. D., Jr., Coop, A., Toth, E. A., and Weber, D. J. (2008) Divalent metal ion complexes of S100B in the absence and presence of pentamidine. *J. Mol. Biol. 382*, 56−73.
(37) Drohat, A. C., Amburgey, J. C., Abildgaard, F., Starich, M. R., Baldisseri, D., and Weber, D. J. (1996) Solution structure of rat apo-S100B($\beta\beta$) as determined by NMR spectroscopy. *Biochemistry 35*, 11577−11588.
(38) Amburgey, J. C., Abildgaard, F., Starich, M. R., Shah, S., Hilt, D. C., and Weber, D. J. (1995) ^{1}H, ^{13}C and ^{15}N NMR assignments and solution secondary structure of rat Apo-S100β. *J. Biomol. NMR 6*, 171−179.
(39) Kabsch, W. (2010) Xds. *Acta Crystallogr. D66*, 125−132.
(40) Soltis, S. M., Cohen, A. E., Deacon, A., Eriksson, T., Gonzalez, A., McPhillips, S., Chui, H., Dunten, P., Hollenbeck, M., Mathews, I., Miller, M., Moorhead, P., Phizackerley, R. P., Smith, C., Song, J., van dem Bedem, H., Ellis, P., Kuhn, P., McPhillips, T., Sauter, N., Sharp, K., Tsyba, I., and Wolf, G. (2008) New paradigm for macromolecular crystallography experiments at SSRL: Automated crystal screening and remote data collection. *Acta Crystallogr. D64*, 1210−1221.
(41) Cohen, A. E., Ellis, P. J., Miller, M. D., Deacon, A. M., and Phizackerley, R. P. (2002) An automated system to mount cryo-cooled protein crystals on a synchrotron beamline, using compact sample cassettes and a small-scale robot. *J. Appl. Crystallogr. 35*, 720−726.
(42) McPhillips, T. M., McPhillips, S. E., Chiu, H. J., Cohen, A. E., Deacon, A. M., Ellis, P. J., Garman, E., Gonzalez, A., Sauter, N. K., Phizackerley, R. P., Soltis, S. M., and Kuhn, P. (2002) Blu-Ice and the Distributed Control System: Software for data acquisition and instrument control at macromolecular crystallography beamlines. *J. Synchrotron Radiat. 9*, 401−406.
(43) Gonzalez, A., and Tsai, Y. (2010) *AUTOXDS*, Stanford University, Stanford, CA.
(44) Leslie, A. G. W., and Powell, H. R. (2007) Processing Diffraction Data with Mosflm. *Evolving Methods for Macromolecular Crystallography 245*, 41−51.
(45) Project, C. C. (1994) The CCP4 Suite: Programs for Protein Crystallography. *Acta Crystallogr. D50*, 760−63.
(46) Gibson, R. P., Tarling, C. A., Roberts, S., Withers, S. G., and Davies, G. J. (2004) The donor subsite of trehalose-6-phosphate synthase: Binary complexes with UDP-glucose and UDP-2-deoxy-2-fluoro-glucose at 2 Å resolution. *J. Biol. Chem. 279*, 1950−1955.
(47) Matsumura, H., Shiba, T., Inoue, T., Harada, S., and Kai, Y. (1998) A novel mode of target recognition suggested by the 2.0 Å structure of holo S100B from bovine brain. *Structure 6*, 233−241.
(48) Mccoy, A. J., Grosse-Kunstleve, R. W., Adams, P. D., Winn, M. D., Storoni, L. C., and Read, R. J. (2007) Phaser crystallographic software. *J. Appl. Crystallogr. 40*, 658−674.
(49) Adams, P. D., Afonine, P. V., Bunkoczi, G., Chen, V. B., Davis, I. W., Echols, N., Headd, J. J., Hung, L. W., Kapral, G. J., Grosse-Kunstleve, R. W., McCoy, A. J., Moriarty, N. W., Oeffner, R., Read, R. J., Richardson, D. C., Richardson, J. S., Terwilliger, T. C., and Zwart, P. H. (2010) PHENIX: A comprehensive Python-based system for macromolecular structure solution. *Acta Crystallogr. D66*, 213−221.
(50) Emsley, P., Lohkamp, B., Scott, W. G., and Cowtan, K. (2010) Features and development of Coot. *Acta Crystallogr. D66*, 486−501.
(51) Afonine, P. V., Grosse-Kunstleve, R. W., and Adams, P. D. (2005) The Phenix Refinement Framework,. *CCP4 Newsletter*, Vol. *42*, Contribution 8, Daresbury Laboratory, Warrington, U.K.
(52) Hartman, K. G., Vitolo, M. I., Pierce, A. D., Fox, J. M., Shapiro, P., Martin, S. S., Wilder, P. T., and Weber, D. J. (2014) Complex Formation between S100B Protein and the p90 Ribosomal S6 Kinase (RSK) in Malignant Melanoma Is Calcium-dependent and Inhibits Extracellular Signal-regulated Kinase (ERK)-mediated Phosphorylation of RSK. *J. Biol. Chem. 289*, 12886−12895.
(53) Bachman, K. E., Sager, J., Cheong, I., Catto, M., Bardelli, A., Park, B. H., Vogelstein, B., Carotti, A., Kinzler, K. W., and Lengauer, C. (2005) Identification of compounds that inhibit growth of 2-amino-1-methyl-6-phenylimidazo(4,5-b)pyridine-resistant cancer cells. *Mol. Cancer Ther. 4*, 1026−1030.
(54) Myers, M. A. (1998) Direct measurement of cell numbers in microtitre plate cultures using the fluorescent dye SYBR green I. *J. Immunol. Methods 212*, 99−103.
(55) Sauna, Z. E., Peng, X. H., Nandigama, K., Tekle, S., and Ambudkar, S. V. (2004) The molecular basis of the action of disulfiram as a modulator of the multidrug resistance-linked ATP binding cassette transporters MDR1 (ABCB1) and MRP1 (ABCC1). *Mol. Pharmacol. 65*, 675−684.
(56) Wilder, P. T., Baldisseri, D. M., Udan, R., Vallely, K. M., and Weber, D. J. (2003) Location of the Zn^{2+}-binding site on S100B as determined by NMR spectroscopy and site-directed mutagenesis. *Biochemistry 42*, 13410−13421.
(57) Wilder, P. T., Varney, K. M., Weiss, M. B., Gitti, R. K., and Weber, D. J. (2005) Solution structure of zinc- and calcium-bound rat S100B as determined by nuclear magnetic resonance spectroscopy. *Biochemistry 44*, 5690−5702.
(58) Cremer, D., Hausen, B. M., and Schmalle, H. W. (1987) Toward a rationalization of the sensitizing potency of substituted p-benzoquinones: Reaction of nucleophiles with p-benzoquinones. *J. Med. Chem. 30*, 1678−1681.
(59) Mather, B. D., Viswanathan, K., Miller, K. M., and Long, T. E. (2006) Michael addition reactions in macromolecular design for emerging technologies. *Prog. Polym. Sci. 31*, 487−531.
(60) Lou, H., Ookhtens, M., Stolz, A., and Kaplowitz, N. (2003) Chelerythrine stimulates GSH transport by rat Mrp2 (Abcc2) expressed in canine kidney cells. *Am. J. Physiol. 285*, G1335−G1344.
(61) Jemal, A., Murray, T., Samuels, A., Ghafoor, A., Ward, E., and Thun, M. J. (2003) Cancer statistics, 2003. *Ca-Cancer J. Clin. 53*, 5−26.
(62) Abraha, H. D., Fuller, L. C., Du Vivier, A. W., Higgins, E. M., and Sherwood, R. A. (1997) Serum S-100 protein: A potentially useful prognostic marker in cutaneous melanoma. *Br. J. Dermatol. 137*, 381−385.
(63) Banfalvi, T., Gilde, K., Gergye, M., Boldizsar, M., Kremmer, T., and Otto, S. (2003) Use of serum S-S-CD and S-100B protein levels to monitor the clinical course of malignant melanoma. *Eur. J. Cancer 39*, 164−169.
(64) Buer, J., Probst, M., Franzke, A., Duensing, S., Haindl, J., Volkenandt, M., Wittke, F., Hoffmann, R., Ganser, A., and Atzpodien, J. (1997) Elevated serum levels of S100 and survival in metastatic malignant melanoma. *Br. J. Cancer 75*, 1373−1376.
(65) Djukanovic, D., Hofmann, U., Sucker, A., Rittgen, W., and Schadendorf, D. (2000) Comparison of S100 protein and MIA protein as serum marker for malignant melanoma. *Anticancer Res. 20*, 2203−2207.
(66) Guo, H. B., Stoffel-Wagner, B., Bierwirth, T., Mezger, J., and Klingmuller, D. (1995) Clinical significance of serum S100 in metastatic malignant melanoma. *Eur. J. Cancer 31A*, 1898−1902.

(67) Karnell, R., von Schoultz, E., Hansson, L. O., Nilsson, B., Arstrand, K., and Kagedal, B. (1997) S100B protein, 5-S-cysteinyldopa and 6-hydroxy-5-methoxyindole-2-carboxylic acid as biochemical markers for survival prognosis in patients with malignant melanoma. *Melanoma Res. 7*, 393−399.
(68) Mohammed, A. A., and Januzzi, J. L., Jr. (2010) Clinical applications of highly sensitive troponin assays. *Cardiol. Rev. 18*, 12−19.
(69) Levine, A. J. (1997) p53, the cellular gatekeeper for growth and division. *Cell 88*, 323−331.
(70) Kohler, J., and Schuler, M. (2014) LUX-Lung 3: Redundancy, toxicity or a major step forward? Afatinib as front-line therapy for patients with metastatic EGFR-mutated lung cancer. *Future Oncol. 10*, 533−540.
(71) Serafimova, I. M., Pufall, M. A., Krishnan, S., Duda, K., Cohen, M. S., Maglathlin, R. L., McFarland, J. M., Miller, R. M., Frodin, M., and Taunton, J. (2012) Reversible targeting of noncatalytic cysteines with chemically tuned electrophiles. *Nat. Chem. Biol. 8*, 471−476.
(72) Erlanson, D. A., Wells, J. A., and Braisted, A. C. (2004) Tethering: Fragment-based drug discovery. *Annu. Rev. Biophys. Biomol. Struct. 33*, 199−223.
(73) Potashman, M. H., and Duggan, M. E. (2009) Covalent modifiers: An orthogonal approach to drug design. *J. Med. Chem. 52*, 1231−1246.
(74) Lim, S. Y., Raftery, M. J., Goyette, J., Hsu, K., and Geczy, C. L. (2009) Oxidative modifications of S100 proteins: Functional regulation by redox. *J. Leukocyte Biol. 86*, 577−587.
(75) Meghnani, V., Vetter, S. W., and Leclerc, E. (2014) RAGE overexpression confers a metastatic phenotype to the WM115 human primary melanoma cell line. *Biochim. Biophys. Acta 1842*, 1017−1027.